

Topology-Aware Surface Reconstruction for Point Clouds

Rickard Brüel Gabrielsson¹ Vignesh Ganapathi-Subramanian¹ Primož Skraba^{2,3} Leonidas J. Guibas¹

¹Stanford University ²Queen Mary University of London ³Jožef Stefan Institute

rbg@cs.stanford.edu, viganusub@stanford.edu, p.skraba@qmul.ac.uk, guibas@cs.stanford.edu

Abstract

We provide an approach to utilize topological priors to reconstruct the surface of a point scan. In particular, we learn parameters for the basis functions that are used for surface reconstruction, satisfying predefined topological constraints. These requirements are captured by persistence diagrams, and these are used to inform the optimization process that learns the parameters. We obtain parameters to build a likelihood function over the reconstruction domain. This novel topology-aware technique is useful to weed out topological noise from point scans, apart from capturing certain nuanced properties of the underlying shape, that could otherwise be lost while performing direct surface reconstruction. We showcase results reconstructing shapes with multiple potential topologies, compare to other classical surface construction techniques and show completion of medical and real scan data.

1. Introduction

Shapes are characterized by a number of markers that are representational, and explain their different aspects. These aspects could be geometric, structural, topological, functional or stylistic. These considerations add to our understanding of shape collections, and can be instrumental in solving important problems in 3D vision, geometry processing and computer graphics like shape alignment, shape correspondences, surface reconstruction and shape synthesis.

Of these different considerations, topology invariance of shapes is an oft-observed trait across collections, that is seldom exploited. Topological invariance is an important property of many collections, especially those where the shapes are built in an organic and similar manner. This can be observed especially in human body parts. Most instances of a certain human body part, owing to the fact that they are all formed in a very similar manner, are homotopic. This is to say that the topology of the human heart is always the same, be it that of a child or an older person.

Most shape processing problems, in particular surface extraction techniques, involve choices that are both contin-

uous and combinatorial. Continuous choices involve parameter regression, where a certain set of parameters can be regressed from within a continuous set. This could include learning chair leg lengths, or radius of a spherical object. The more difficult combinatorial or discrete choices are those that involve making type classification decisions on shapes. This is seen very often in regressing shape grammars, where an example of a combinatorial choice is that of having an armrest or not. These combinatorial choices are extremely challenging to make, and prove to be a bottleneck in many shape processing tasks.

Persistent homology is a tool that provides us topological markers that capture these combinatorial choices by means of a continuous proxy. Persistence diagrams capture multi-scale topology of data. Surface extraction from a point scan usually involves being oblivious to the scale of the point scan, and this could lead to topologically incorrect reconstructions. Here, we provide a technique where we extract a surface from a point scan, preserving the predefined topology of the shape. Since persistence-based tools range across different scales, we manage to sieve out a reliable reconstruction of the point scan respecting the requisite topology.

Most surface extraction techniques that utilize topological information, treat it as post-processing data. We attempt to build likelihood functions that take high values on points that likely lie on the surface. These functions are informed by backpropagation from the persistence diagrams of candidate surfaces, aiding to obtain one of requisite topology. These diagrams act as an intermediary between continuous scale information around the points of the point scan, and the combinatorial aspect which topology aims to capture.

Utilization of topological information for point scan completion can aid in completing sparse point scans reliably. This can also be useful for resolving topological ambiguities that arise from the incomplete nature of point scans, especially in the case of non-intersecting close regions on the surface of the shape. These advantages of topology-aware shape completion shall be showcased with multiple examples in Section 8.

In summary, the contributions of this work are as below:

- A novel topology-aware likelihood function, learned

on a point cloud based on persistent homology measures of any dimension.

- A completely automated surface extraction algorithm that preserves or even creates requisite topology.
- State-of-the-art results of topological fidelity in reconstruction.
- A novel metric that measures quality of surface reconstruction.

2. Related Work

Performing surface reconstruction from point clouds is a very well-studied and open problem, and in this paper, we attempt to use topological markers to perform this surface reconstruction in a topology-aware manner. In this section, we list important related works that have been critical in understanding and expanding these research ideas.

2.1. Persistent Homology

Using topological markers to inform shapes has been performed in different forms for a long time. Persistence has served to be a valuable bridge between problems that employ optimization on a continuous and often compact spaces, as opposed to performing combinatorial optimizations. Persistence has aided to solve topological simplification based issues while performing functional optimization [12]. In general, persistence has been used as a tool to satisfy topological criteria in a variety of geometry processing applications such as shape matching [7], optimal pose-matching [10] and shape segmentation [31].

The problem of attempting to perform topological simplification of shapes as in the context of preserving persistent features in given data has traditionally been performed in the context of function denoising [1, 3]. The work of Gameiro et al. [13] where the authors attempt to continue a point cloud for dynamical systems based applications. Recent work by Poulenard et al. [25], use the idea of function optimization for the purpose of shape matching. The work in this paper mirrors that of Poulenard et al., by performing function optimization on basis coefficients, which are used to be building blocks of a given function, which in this case is representative of the shape surface.

2.2. Surface Reconstruction from Point Clouds

Surface extraction is a well-studied problem, and we shall list a set of relevant related works in this section. Since the problem of surface reconstruction has multiple facets and many interesting sub-problems, we direct the reader to check the survey by Berger et al. [5] for further reading.

There are three major scenarios where surface reconstruction from point clouds is performed, mainly those of urban reconstruction [22], completing partial surfaces or

point scans [2] and interpolating a point cloud to generate an entire surface [16, 9]. In our paper, we mainly consider the third problem, where space, and the surface it contains, are characterized by a function and its properties.

Most surface extraction techniques model the surface to be characterized by the zero-level set of a function that is defined over space [19, 8, 27]. These works approximate the signed Euclidean distance from the underlying surface, and essentially interpolate values between the input points, extracting the underlying surface as a zero set of this interpolated distance field. Since there is no additional information in this sort of technique, there is nothing to prevent points far from the surface to have extremely low values. Therefore, most techniques obtaining reasonable results use an *inside-outside points* approach, where points inside the surface and outside it, are provided so as to guide the function sign at various regions in space. Moreover, while this is an extremely elegant representation of a shape, it is also very restrictive, with multiple equality constraints being solved for during the optimization step. The work by Poranne et al. [24] takes a minor detour from this, where they don't necessarily force the surface value to be zero. Instead, they obtain the surface by applying an algorithm based on the watershed transform [26], that pulls out the low-level set of the function values as the surface. In this work we build a likelihood function where points on the surface are given high values, with no value constraints. This way, the surface values can develop organically. A simple surface extraction technique from existing function values can be used to obtain the actual surface.

Topological control in surface reconstruction has been performed by user interaction [29, 33], fixed template optimization [4, 14, 34], removing topological errors from an existing surface [18, 32] and optimization-based algorithmic surface reconstruction [28, 17, 35, 20]. In this work, we approach the topology-guided reconstruction along the lines of the optimization-based technique, learning parameters that maximize the function values at surface points, while preserving the topology, using ideas from persistent homology as discussed in Section 2.1.

3. Overview

The rest of the paper is arranged as follows. In Section 4, the idea of persistence is reviewed. A discussion of classical surface reconstruction is included in Section 5, and the two ideas are organically put together to perform topology-aware surface reconstruction. In Section 6, the optimization to build a topology-aware likelihood function is discussed. This is extended in Section 7, where an extraction technique to obtain a surface from the likelihood function is provided. Section 8 showcases the technique in practical example cases, and evaluates it against other state-of-the-art reconstruction techniques. Section 9 concludes the paper

with a brief discussion on future work.

4. Persistence Diagrams

We begin with a brief discussion on persistent homology, persistence diagrams, and how they are computed [7, 6]. We refer the reader to [11] for a more in depth description. Taking in an increasing sequence of spaces as input, persistent homology tracks how topological features appear and disappear in this sequence. While the formal definition is algebraic, for our purposes we are concerned only with the 0, 1, and 2-dimensional homology groups (which in our setting are vector spaces). These vector spaces capture aspects of connectedness and holes in the underlying data, with the dimension of 0-dimensional homology counting the number of connected components, 1-dimensional homology capturing the number of holes, and 2-dimensional homology capturing the number of voids.

We represent a space by a geometric realization of a *simplicial complex*, K . Each k -dimensional simplex is the convex combination of $k+1$ vertices. While not required by the method, in this paper we assume that K is embedded and is a triangulation of a subset of Euclidean space (though we restrict ourselves to dimensions 2 and 3). We remark that the method is more general and can be applied to representations such as cubical complexes (which are equivalent to pixels and voxels).

In addition to a complex, we assume that we are given a function $f : K \rightarrow \mathbb{R}$. Given f , we can define a filtration \mathcal{F} as a sequence of super-level sets (resp. sub-level sets) of f .

$$K^\alpha = f^{-1}[\alpha, \infty)$$

The only condition on the function is that it is *monotone* [11], for every α , K^α is also a simplicial complex.

Corresponding to \mathcal{F} , it is possible to draw a persistence diagram (see Figure 1), which describes how components, holes, and voids evolve as α changes. A persistence diagram contains points for each dimension of topological features (equivalently, there is a persistence diagram for each dimension), where each point has coordinates which are called birth and death times (b_i, d_i) . The birth time represents the appearance of a k -dimensional hole (a component is a 0-dimensional hole) and the death represents when this hole gets filled in (for connected components, this represents the merging of two components).

There are numerous algorithms and implements for computing persistence diagrams efficiently and we direct the reader to [23]. In practice, rather than general super-level set filtrations on simplicial complexes, we consider upper-star filtrations, where all the function values occur at vertices. Following [25], one can view the persistence diagram as a map taking the underlying space K and a function g to a set of points in \mathbb{R}^2 . Letting \mathcal{I} denote the index on points

in the persistence diagram, the map can be defined as:

$$P_g : (K, f) \rightarrow \{(b_i, d_i)\}_{i \in \mathcal{I}} \quad (1)$$

Furthermore, since we assume our complex is embedded, the vertices of K are points \mathcal{X} in the ambient space (in our examples, usually \mathbb{R}^2 or \mathbb{R}^3). For every function on the points $f : \mathcal{X} \rightarrow \mathbb{R}$, we can linearly extend it to a function g on K , where

$$g(\sigma) = \max_{v \in \sigma} f(v)$$

Hence, we can view the persistence diagram as a map

$$P_f : (\mathcal{X}, f, K) \rightarrow \{(b_i, d_i)\}_{i \in \mathcal{I}}$$

where we assume a fixed underlying simplicial complex.

5. Implicit Surface Representation

If we consider a set of basis functions φ_p that is defined around every point in a point cloud, $p \in \mathcal{P}$ and let each function be parameterized by α_p . We attempt to model the surface covering the points in \mathcal{P} as a combination of these basis functions.

$$f(p, \alpha_{\mathcal{P}}) = \sum_{p \in \mathcal{P}} \varphi(\alpha_p) \quad (2)$$

In the above notation, $\alpha_{\mathcal{P}}$ refers to the set of all α_p parameters for all points $p \in \mathcal{P}$, or $\alpha_{\mathcal{P}} = \cup_{p \in \mathcal{P}} \alpha_p$. If we require every point on the surface to evaluate to 0, this can be used to extrapolate the unknown surface from the known points on the scan. The choice of basis functions φ_p are a design choice, and would ideally be functions that would evaluate to 0 at the point p around which they are centered. This approach has been used effectively in the past to perform surface reconstruction from point scans [19, 8].

We use the framework from [25] to determine how the parameters $\alpha_{\mathcal{P}}$ influence the persistence diagram, and back-propagate information from the persistence diagram to the function $f(\cdot, \alpha_{\mathcal{P}})$ down to the parameters $\alpha_{\mathcal{P}}$.

Classical surface reconstruction techniques use different tricks to build a function to fit a surface to a point scan. Poisson reconstruction attempts to perform this by evaluating a function to 0 on the surface and 1 elsewhere. This inside-outside description of points, along with some extra information such as normal information can be used to then reduce the problem to solving the Poisson equation [19]. Another approach using radial-basis functions, again evaluates to 0 on the surface and a small value at nearby points not on the surface [8]. In our approach, we attempt to build the surface to be higher-valued as opposed to lower-valued as in the above two techniques. We construct Gaussians centered around the points on the scan, and try to maximize the value around the point scans. We then use a topology-aware

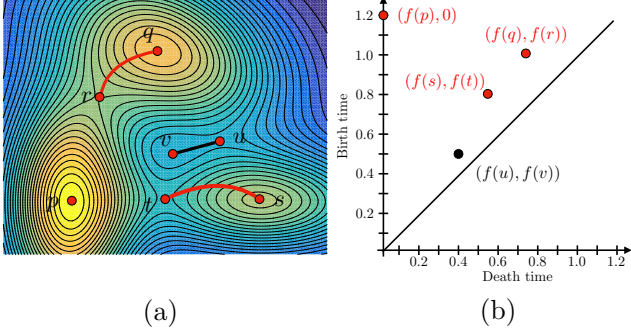


Figure 1. An example of a persistence diagram for the sum of 3 Gaussians in 2D. (a) Heat map of the function (b) The corresponding persistence diagram. The critical points of the height function p, q , and s are local maxima, r, t , and u are saddles and v is a local minima. Each of the local maxima create a component (the red points on the right represent 0D homology classes – the heights are the birth times). Saddles r and t merge components and so they correspond to the death times of two of the red points. The saddle u creates a hole (1D homology class), which is closed when the minima at v is reached – corresponding to the black point in (b).

surface extraction technique to obtain the surface from this maximal function built over the point scans.

A multivariate 3-D Gaussian at a point x is given by

$$G(x; \mu, \Sigma) = \sqrt{(2\pi)^{-3} |\Sigma|^{-1}} \exp(-(x - \mu)^T \Sigma^{-1} (x - \mu))$$

Here Σ is a symmetric covariance matrix. In our setup, we define the Gaussian basis-function around point p of \mathcal{P} to be $\varphi_p(x; \alpha_p) = G(x; p, \alpha_p^T \alpha_p)$. The Gaussian, as described earlier, is centered around the point on the scan p . The covariance matrix of a Gaussian describes the reach of the Gaussian, and is known to be a symmetric positive-definite matrix. Since every symmetric positive definite matrix M can be decomposed into the form $M = A^T A$ for some matrix A . This matrix A is also called the square root matrix of M . Mathematically, if the singular value decomposition (SVD) of M is given by $M = U \Lambda U^T$, defining A to be $A = U \Lambda^{0.5} U^T$ satisfies $M = A^T A$. Note that if $\Lambda = \text{diag}(\lambda_1, \lambda_2, \lambda_3)$, $\Lambda^{0.5} = \text{diag}(\sqrt{\lambda_1}, \sqrt{\lambda_2}, \sqrt{\lambda_3})$ (square roots of singular values of M). We define our parameters matrix α_p to be this square root matrix, that is the building block of the covariance matrix.

The likelihood functions provide a solid heuristic to initialize our variables and we also sample grid-points from them. Usually the covariance is initialized such that the derivative of the Gaussian is maximized at the average distance between points.

It is also important to define the domain of the function f which we use to define the filtration. We consider a grid, with the function being evaluated at all grid points. The resolution of the grid ensures non-trivial distances between points in the point cloud and the grid points. The underlying

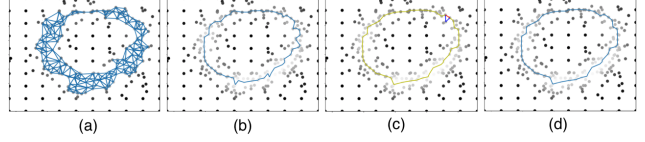


Figure 2. Steps of the Surface Extraction algorithm. (a) Simplicial complex (b) Generator/Proposed surface (c) Enumerating intersecting cofaces (d) 1D surface output

simplicial complex is a triangulation of the grid.

6. Topology-aware Optimization

Our optimization procedure assumes that we have some a priori information about the topology of our surface. Determining the topology from a point cloud is a related but separate problem, which we do not address in this work.

Topological priors can take several different forms. For example, it takes the form of the number of components, holes, or voids that we would like the reconstructed surface to have or it could even be a more general prior, eg. multiple voids are present. More specifically, we assume that the k -most persistent features of the 1-dimensional homology are required to be present in the reconstructed shape. An example objective function that we consider for this is to maximize the persistence of the k -most persistent points in the persistence diagram. Sorting the points by persistence, we optimize using the energy functional

$$\mathcal{F}_{\text{top}} = - \sum_{i=1}^k (d_i - b_i)^2$$

Poulenard et al. [25] show how the derivatives of birth and death components can be computed with respect to parameters on which the persistence diagrams depend. In a similar approach, we build our filtration by considering grid points $x \in \mathcal{X}$. It is possible to build a unique map $\pi = (\pi_b, \pi_d)$ (if the grid point function values are unique) from the set of points in the persistence diagram to pairs of grid points $(x_b, x_d) \in \mathcal{X} \times \mathcal{X}$. Again following the same approach as [25], we can compute the gradient as

$$\nabla_{\alpha_p} b_i = \nabla_{\alpha_p} f(x_{b,i}, \alpha_p),$$

and

$$\nabla_{\alpha_p} d_i = \nabla_{\alpha_p} f(x_{d,i}, \alpha_p),$$

where $x_{b,i} = \pi_b(b_i)$ and $x_{d,i} = \pi_d(d_i)$. Combining the terms, the gradient of the energy functional is:

$$\nabla_{\alpha_p} \mathcal{F}_{\text{top}} = \sum_{i=1}^k 2(b_i - d_i) \nabla_{\alpha_p} (b_i - d_i) \quad (3)$$

Since $\nabla_{\alpha_p} (b_i - d_i) = \nabla_{\alpha_p} (f(x_{b,i}, \alpha_p) - f(x_{d,i}, \alpha_p))$, the gradient can be computed using the gradient of the Gaussian:

$$f(x_{b,i}, \alpha_p) = \sum_{p \in \mathcal{P}} G(x_{b,i}; p, \alpha_p^T \alpha_p).$$

Therefore,

$$\nabla_{\alpha_p} f(x_{b,i}, \alpha_p) = -\alpha_p((\alpha_p^T \alpha_p)^{-1} - (\alpha_p^T \alpha_p)^{-1}(p - x_{b,i})(p - x_{b,i})^T(\alpha_p^T \alpha_p)^{-1}),$$

which gives:

$$\nabla_{\alpha_p} \mathcal{F}_{\text{top}} = \alpha_p^{-T} \left(\sum_{i=1}^k D(p, x_{b,i}, x_{d,i}, b_i, d_i) \right) (\alpha_p^T \alpha_p)^{-1} \quad (4)$$

with

$$D(p, x_{b,i}, x_{d,i}, b_i, d_i) = 2(b_i - d_i)((p - x_{d,i})(p - x_{d,i})^T - (p - x_{b,i})(p - x_{b,i})^T).$$

We implemented the entire module in PyTorch and would make the code publicly available on acceptance. Note that the cost function showcased above is an example, and other such differentiable functions can be used instead. In the implementation, backpropagation is separated for the diagrams; therefore one could add custom cost functions.

7. Surface Extraction

Our objective is to fit a likelihood function to a surface with a desired topology, with the function value large on the surface. If constraints allow, we want low variance as to be certain about the position of the surface. The persistence framework works on a simplicial complex, in our case a type of top-level set, and our optimization aims at securing a simplicial complex at a certain filtration value (or a top-level set for a certain function value) with the prerequisite topology. Ideally, this simplicial complex has few boundary elements which is roughly equivalent to a small top-level set. This simplicial complex could be thought of as a set of candidate surfaces achieving the desired topology, and which can be made smaller or even reduced to one candidate if enough constraints (topological or other) are added. In many cases, one merely wants high-level topological constraints and it is crucial to allow for such flexibility.

The output of our optimization process is a likelihood function that is large where the surface should be and where the surface has the desired topology. From this we can pick the filtration- or function value for which the top-level set achieves the desired topology. Therefore, we often visualize the simplicial complex or top-level set with the guaranteed topology, which in many ways is equivalent to a voxel-surface with the correct topology.

There are multiple ways to extract a 1D or 2D surface. One could apply the watershed algorithm [24] to the inverse of our likelihood function. Of course, this cannot guarantee the topology of the result. However, a natural extension to our work is to use the generators of the persistent homologies we are optimizing for as proposals that may in-

creamentally be improved using the boundaries of our simplicial complex. This allows us to extract a 1D or 2D surface while guaranteeing the topology of the output. Specifically, one can obtain a bijective correspondence between the simplices in the filtration to the homology generators, providing a birth-death pairing to every homology generator - except for those persisting to infinity [15, Theorem 2.3]. This generator has the correct topology and consists of simplices within the optimized simplicial complex. However, it might not be the best candidate considering other information. Typically, the generator has intersecting co-faces within the simplicial complex (i.e. its boundary) and by iterating over intersecting co-faces we can consider adding the co-face (or boundary element) to our generator to get a new generator with the correct topology. Thus, one can define a local function over a face of the generator and intersecting co-faces to locally optimize the surface. For example, one function we optimized for (in the 1D surface case) considered an edge (a, b) on the proposed surface, and each intersecting boundary element (a, b, c) , and added the boundary element if $f(c) > \max(f(a), f(b))$ and (b, c) was not an edge on the proposed surface, else it added the boundary element if $f(c) < \max(f(a), f(b))$. In the first case we add an edge, and in the second case we remove an edge. This function was constructed as to encourage the removal of edges since the number of edges was considered to be a proxy for smoothness. In this process, we also, to maintain the topology, disallowed any co-faces that would cause the surface to self-intersect, and the process stops when no further co-faces can be added/dropped. This algorithm extends naturally to 2D surfaces. A simple example of the algorithm can be seen in Figure 2.

8. Results

Our topology-aware surface reconstruction is a novel technique; the only technique that guarantees the requested topology while incorporating surface reconstruction, while providing flexibility for different topological reconstructions. All other topology-aware surface reconstruction techniques, as discussed in Section 2, use heuristics to approximate topological constraints, and optimize objective functions that respect these heuristics. Our technique is also alone in accepting topological information of any dimension. In this section, we discuss multiple results that validate our technique, and compare it to other state-of-the-art surface reconstruction techniques.

8.1. Topological Guarantee

As discussed earlier, the biggest advantage of our technique over other existing ones is the topological guarantee it provides. This aids in it being a fantastic initialization for other reconstruction techniques that require topological fidelity, but cannot guarantee one. Our technique is unique

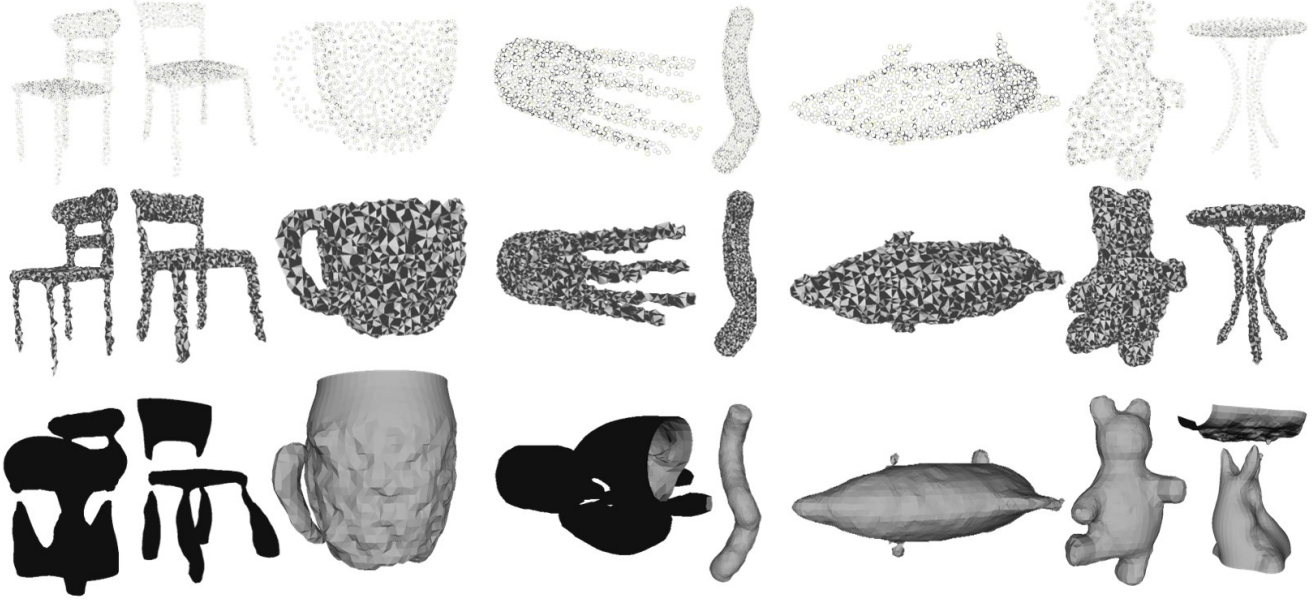


Figure 3. Reconstruction of example point clouds from the McGill dataset [30]. *First row:* Input Point cloud *Second row:* Our reconstruction of the shape in the first row. *Third row:* Poisson surface reconstruction [19] of the shape in the first row. Shapes showcased (left to right) are two chairs, cup, octopus, snake, dolphin, teddy and table respectively.

in this aspect, since no previous technique has managed to provide this sort of topological guarantee in surface reconstruction. In Figure 4, we see that a spider can be reconstructed to have one void or two. Most surface reconstruction techniques provide one major void, while the other is flattened out, while in our case, we can force this second void by means of pre-defining the requisite topology.

This topological guarantee can be further exemplified in the ring as shown in Figure 5. This is a two-dimensional case, with a point cloud as shown in Figure 5(a). Now, the sampling makes it ambiguous about the source shape containing one hole or two. But if this information is available, then our technique can be utilized to reconstruct the ring accordingly as in Figure 5(b) and (c) respectively. Most surface reconstruction technique use tangent and normal information of points to reconstruct the underlying surface from them. In this case, though, that would mean that the reconstruction with one hole would almost always be produced. So having the underlying topology at hand beforehand, would help in this case.

Another example where this is showcased is in that of the steering wheel in Figure 6. Here, different topologies (3, 2 or 1 rings) are used to reconstruct an input point cloud, and the reconstructions are vastly different from each other. It is observed that for each of the different topologies, the technique progressively closes the less persistent void. It is to be noted that by equipping the technique with topological preservation as a very important criterion, the technique is able to obtain reconstructions, that are seemingly very far off from the original point cloud or surface as in Figure 6(a)

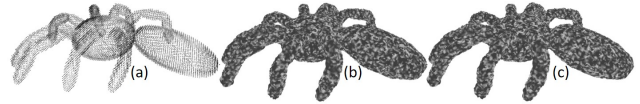


Figure 4. Reconstructing spider model with multiple possible topologies. (a) Input spider point cloud. (b) Creating 1 void inside the spider (c) Creating 2 voids inside the spider (note the swollen central lobe of the spider)

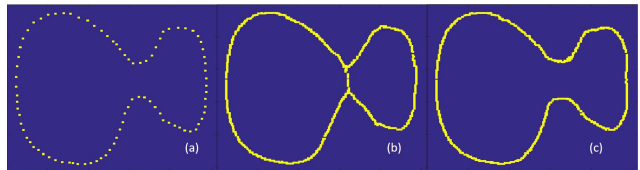


Figure 5. Reconstructing dual circle with multiple possible topologies. (a) The 2-D dual circle point cloud. (b) Reconstruction of merged dual circle with one hole (c) Reconstruction of dual circle as two adjacent circles

and (b), but respect topological requirements.

8.2. Shape Completion

Shape completion is an important problem that we tackle from a topological perspective. Since this sort of treatment, with guaranteed topology has never been attempted to perform shape completion from partial point scans or voxel grids, we claim uniqueness in this aspect.

We perform this in both 2-dimensional and 3-dimensional cases. We show how an incomplete face as shown in Figure 7 is completed by means of our technique.

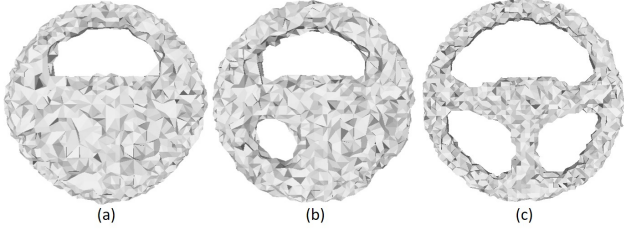


Figure 6. Reconstruction of steering wheel with multiple void topologies. (a) 1 void (b) 2 voids (c) 3 voids

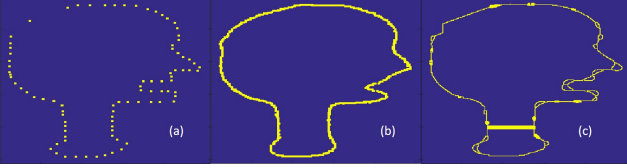


Figure 7. (a) 2-D incomplete head point cloud (b) Completing the point cloud with topological information (1-hole) (c) Using the generalized distance based watershed algorithm as in Poranne et al. [24] to complete the point cloud.

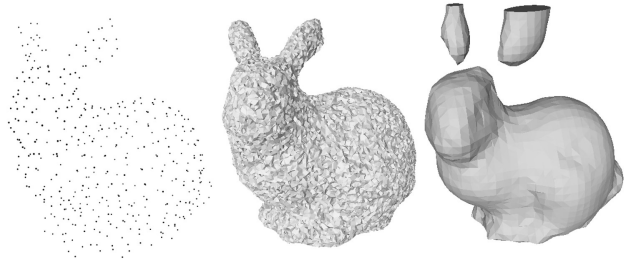


Figure 8. Densifying the Stanford bunny. (a) A sparse point cloud sampled from the Stanford bunny. (b) Reconstruction of this sampling, preserving only the essential 2-dim hole (c) Poisson reconstruction of the sparse Stanford bunny.

Here, the topology of the face, with a hole is provided as the only input apart from the input point cloud, and the technique performs the completion accordingly. It is also seen here, that using the reconstruction technique described in Poranne et al. [24], captures the high level structure of the shape, introduces a lot of topological noise.

Another example where we showcase the completion power of our technique is when sparse sampling introduce topological ambiguity. In Figure 8(a), where there are too few points in the input point cloud, attempting to reconstruct this with a single 2-dimensional hole, enforces the reconstruction to produce a consistent, bunny-like reconstruction. This is not necessarily the case when other reconstruction techniques are used. Here, we showcase the Poisson surface reconstruction of the sparse Stanford bunny in Figure 8(c), it can be seen that the sparsity of the point cloud provides three major concentrations of points in the shape, therefore getting a topologically wrong reconstruction.

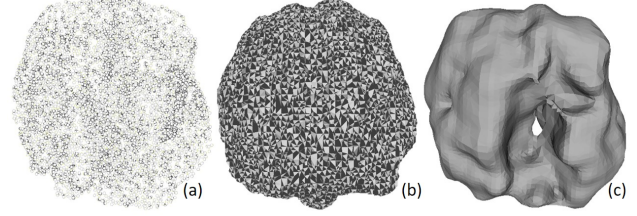


Figure 9. Reconstruction of the human brain as seen from the top-view. (a) A point cloud of an example brain from Lerma-Usabiaga et al. [21]. (b) Reconstruction of this brain, preserving two central voids. (c) Poisson Reconstruction of the brain.

8.3. Medical Data

The central motivation to obtain topology-aware surfaces is the potential application to medical data. As described in Section 1, topology of medical data is always predefined, and is invariant across various instances. This is a central property that can be utilized, along with other medical priors, to reconstruct various medical organs from scan data.

To showcase this, we show examples of how one could use this to reconstruct scans of different medical organs. In Figure 9, we observe the reconstruction of the brain from the the scan data provided in Lerma-Usabiaga et al. [21]. In this case, it can be noticed that even though the input point cloud is dense, it is fairly complex to reconstruct. While our technique reconstructs the brain fairly close to the input point cloud, the more classical Poisson surface reconstruction [19] fails to obtain a topologically correct reconstruction, producing a one-dimensional hole, while the correct topology would consist of two two-dimensional voids, one for each hemisphere of the brain.

We also attempt to reconstruct synthetic point clouds of human hearts. Human heart scans are widely captured, though restricted in availability, and the topology of the human heart is very complex. This makes our method valuable for reconstruction; we showcase this reconstruction in Figure 10. Here, it is seen that while our method reconstructs the four openings in the human heart, the Poisson reconstruction smoothens the holes, changing the topology of the reconstructed surface.

8.4. Comparisons to other Surface Reconstruction/Extraction techniques

Here, we compare our topology-aware technique to two major surface reconstruction techniques. For 2-D surface extraction, we shall compare our technique to that of Poranne et al. [24], and for 3-D surface reconstruction, we compare primarily to Poisson surface reconstruction [19]. These qualitative comparisons are seen in Figures 7 and 3. While the Poisson reconstruction is very good on smooth water-tight surfaces, it tends to fail for more natural cases where the inherent topology is non-manifold. This is ob-

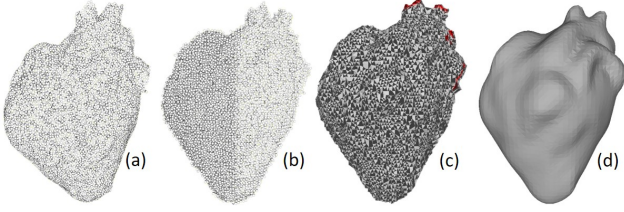


Figure 10. Reconstruction of the human heart model. (a) A point cloud of a human heart model. (b) Reconstruction (point cloud) of this heart model with four openings (2 openings on the top, and 2 on the sides). (c) Same reconstruction as in (b), in mesh form. The red markings here indicate the four holes in the reconstruction. (d) Poisson Reconstruction of the heart.

served in the non-manifold examples of Figure 3 such as chair, cup, octopus and table examples, where the Poisson reconstruction attempts to obtain a water-tight surface and fails both topologically and in reconstruction quality. We perform our 2-D quantitative comparison experiments on the 2-D point clouds used in Poranne et al. [24], specifically the *hand, spiral, helix, face, circle* and *blob* datasets, and the 3-D comparisons on 8 categories of the McGill segmentation benchmark dataset [30].

We develop two different metrics to compare against existing algorithms. We compare against Poisson surface reconstruction [19] for 3D reconstruction and Generalized distance based reconstruction [24] for both 2D and 3D reconstruction. Since our technique aims at perfecting topological accuracy, we compare against the topological accuracy of other techniques. This is done by computing the average number of erroneous k -dimensional components: $\text{TFI}_k = \frac{1}{N} \sum_{i=1}^N |n_{i,k} - n_{i,k}^{\text{recon}}|$, where N refers to the number of shapes. We refer to TFI_k as the k -dimensional Topological Fidelity Index. Here, if $k = 1$, then $n_{i,1}$ is the number of true 1-D holes in shape i , $n_{i,k}^{\text{recons}}$ refers to the number of 1-D holes in the reconstruction of shape i . We showcase this for multiple scan sizes of our input point cloud. This is showcased in Table 1. Our topological guarantee ensures a TFI of 0 for our technique, while a bigger TFI value for other techniques is a measure of how far from ideal their reconstruction capabilities are topologically. The high TFI values for both other methods shows the value of our method that provides topological guarantee.

While the TFI captures topological fidelity, another important factor is the quality of reconstruction. To capture this, we compute the one-way Chamfer distance between a point cloud and its reconstruction. This score is normalized for all shapes in a collection and averaged over the collection. The comparison of these scores across the corresponding techniques for 2D and 3D is provided in Table 2. Here, we show that, our technique, in addition to perfect topological fidelity, also obtains high quality surface reconstruction.

Method - 2D	$N = 1000$	$N = 500$	$N = 200$
Ours ($k=0$)	0	0	0
Watershed [24]	0.25	0.33	0.81
Ours ($k=1$)	0	0	0
Watershed	2.25	3.08	3.63
Method - 3D	$N = 1000$	$N = 500$	$N = 200$
Ours ($k=0$)	0	0	0
Watershed [24]	0.25	0.375	0.375
Poisson [19]	0.75	1.125	0.25
Ours ($k=1$)	0	0	0
Watershed	1.625	2	2.125
Poisson	0.875	0.875	0.875
Ours ($k=2$)	0	0	0
Watershed	0.375	0.375	0.375
Poisson	0.5	0.5	0.625

Table 1. TFI_0 , TFI_1 (and TFI_2) for 2-D (and 3-D) surface reconstruction comparing our technique to the generalized-distance Watershed algorithm by Poranne et al. [24] (and the Poisson surface reconstruction by Kazhdan et al. [19] respectively) for point clouds of size N points. The lowest values are captured in bold.

Method - 2D	$N = 1000$	$N = 500$	$N = 200$
Ours	1.0040	1.0026	0.9979
Watershed [24]	1.0363	1.0479	1.0723
Method - 3D	$N = 1000$	$N = 500$	$N = 200$
Ours	1.9170	1.9143	1.9127
Watershed [24]	1.9867	1.9828	1.9800
Poisson [19]	2.0348	2.0309	2.0117

Table 2. One-way Chamfer distance for 2-D (and 3-D) surface reconstruction comparing our technique to the generalized-distance Watershed algorithm [24] (and the Poisson surface reconstruction [19] respectively) for point clouds of size N points. The lowest values are captured in bold.

9. Conclusion and Future Work

Topology-aware processing is an unexplored, but important aspect to understanding shapes. In this work, we provide a technique that optimizes topology while attempting to perform surface extraction from point scans. With the increasing number of real world scans, this work is very relevant, and crucial to processing shape collections.

As only single scan reconstructions are addressed in this work, one potential direction to proceed would be to learn topological markers from a collection. Often, shape categories in collections share many topological properties, and utilizing this to learn from the data would be valuable. Obtaining topologically correct reconstructions that can still preserve the smooth regularity of natural surfaces is an open challenge. It would also be very useful to utilize topological priors to perform scan reconstruction on medical data.

10. Acknowledgements

Supported by the Slovenian Research Agency (ARRS N1-0058) and by the EU H2020-MSCA-RISE project RENOIR (grant no. 691152). We would like to acknowledge the help of Garikoitz Lerma Usabiaga for his help in understanding brain scan data and manipulating it through the Freesurfer software.

References

- [1] D. Attali, M. Glisse, S. Hornus, F. Lazarus, and D. Morozov. Persistence-sensitive simplification of functions on surfaces in linear time. *Presented at TOPOINVIS*, 9:23–24, 2009. 2
- [2] M. Attene, M. Campen, and L. Kobbelt. Polygon mesh repairing: An application perspective. *ACM Computing Surveys (CSUR)*, 45(2):15, 2013. 2
- [3] U. Bauer, C. Lange, and M. Wardetzky. Optimal topological simplification of discrete functions on surfaces. *Discrete & Computational Geometry*, 47(2):347–377, 2012. 2
- [4] P.-L. Bazin and D. L. Pham. Topology preserving tissue classification with fast marching and topology templates. In *Biennial International Conference on Information Processing in Medical Imaging*, pages 234–245. Springer, 2005. 2
- [5] M. Berger, A. Tagliasacchi, L. Seversky, P. Alliez, J. Levine, A. Sharf, and C. Silva. State of the art in surface reconstruction from point clouds. In *EUROGRAPHICS star reports*, volume 1, pages 161–185, 2014. 2
- [6] G. Carlsson. Topology and data. *Bulletin of the American Mathematical Society*, 46(2):255–308, 2009. 3
- [7] G. Carlsson, A. Zomorodian, A. Collins, and L. J. Guibas. Persistence barcodes for shapes. *International Journal of Shape Modeling*, 11(02):149–187, 2005. 2, 3
- [8] J. C. Carr, R. K. Beatson, J. B. Cherrie, T. J. Mitchell, W. R. Fright, B. C. McCallum, and T. R. Evans. Reconstruction and representation of 3d objects with radial basis functions. In *Proceedings of the 28th annual conference on Computer graphics and interactive techniques*, pages 67–76. ACM, 2001. 2, 3
- [9] T. K. Dey. *Curve and surface reconstruction: algorithms with mathematical analysis*, volume 23. Cambridge University Press, 2006. 2
- [10] T. K. Dey, K. Li, C. Luo, P. Ranjan, I. Safa, and Y. Wang. Persistent heat signature for pose-oblivious matching of incomplete models. In *Computer Graphics Forum*, volume 29, pages 1545–1554. Wiley Online Library, 2010. 2
- [11] H. Edelsbrunner and J. Harer. *Computational Topology - an Introduction*. American Mathematical Society, 2010. 3
- [12] H. Edelsbrunner, D. Letscher, and A. Zomorodian. Topological persistence and simplification. In *Foundations of Computer Science, 2000. Proceedings. 41st Annual Symposium on*, pages 454–463. IEEE, 2000. 2
- [13] M. Gameiro, Y. Hiraoka, and I. Obayashi. Continuation of point clouds via persistence diagrams. *Physica D: Nonlinear Phenomena*, 334:118–132, 2016. 2
- [14] V. Ganapathi-Subramanian, O. Diamanti, S. Pirk, C. Tang, M. Nießner, and L. J. Guibas. Parsing geometry using structure-aware shape templates. *CoRR*, abs/1808.01337, 2018. 2
- [15] R. Ghrist. Barcodes: the persistent topology of data. *Bulletin of the American Mathematical Society*, 45(1):61–75, 2008. 5
- [16] G. Guennebaud and M. Gross. Algebraic point set surfaces. In *ACM Transactions on Graphics (TOG)*, volume 26, page 23. ACM, 2007. 2
- [17] Z. Huang, M. Zou, N. Carr, and T. Ju. Topology-controlled reconstruction of multi-labelled domains from cross-sections. *ACM Transactions on Graphics (TOG)*, 36(4):76, 2017. 2
- [18] T. Ju, Q.-Y. Zhou, and S.-M. Hu. Editing the topology of 3d models by sketching. *ACM Transactions on Graphics (TOG)*, 26(3):42, 2007. 2
- [19] M. Kazhdan, M. Bolitho, and H. Hoppe. Poisson surface reconstruction. *Indicator*, 1(1):0, 2006. 2, 3, 6, 7, 8
- [20] R. Lazar, N. Dym, Y. Kushinsky, Z. Huang, T. Ju, and Y. Lipman. Robust optimization for topological surface reconstruction. *ACM Trans. Graph.*, 37(4):46:1–46:10, July 2018. 2
- [21] G. Lerma-Usabiaga, M. Carreiras, and P. M. Paz-Alonso. Converging evidence for functional and structural segregation within the left ventral occipitotemporal cortex in reading. *Proceedings of the National Academy of Sciences*, 115(42):E9981–E9990, 2018. 7
- [22] P. Musialski, P. Wonka, D. G. Aliaga, M. Wimmer, L. Van Gool, and W. Purgathofer. A survey of urban reconstruction. In *Computer graphics forum*, volume 32, pages 146–177. Wiley Online Library, 2013. 2
- [23] N. Otter, M. A. Porter, U. Tillmann, P. Grindrod, and H. A. Harrington. A roadmap for the computation of persistent homology. *EPJ Data Science*, 6(1):17, 2017. 3
- [24] R. Poranne, C. Gotsman, and D. Keren. 3d surface reconstruction using a generalized distance function. In

- Computer Graphics Forum*, volume 29, pages 2479–2491. Wiley Online Library, 2010. 2, 5, 7, 8
- [25] A. Poulenard, P. Skraba, and M. Ovsjanikov. Topological function optimization for continuous shape matching. In *Computer Graphics Forum*, volume 37, pages 13–25. Wiley Online Library, 2018. 2, 3, 4
 - [26] J. B. Roerdink and A. Meijster. The watershed transform: Definitions, algorithms and parallelization strategies. *Fundamenta informaticae*, 41(1, 2):187–228, 2000. 2
 - [27] M. Samozino, M. Alexa, P. Alliez, and M. Yvinec. *Reconstruction with Voronoi centered radial basis functions*. PhD thesis, INRIA, 2006. 2
 - [28] A. Sharf, T. Lewiner, A. Shamir, L. Kobbelt, and D. Cohen-Or. Competing fronts for coarse-to-fine surface reconstruction. In *Computer Graphics Forum*, volume 25, pages 389–398. Wiley Online Library, 2006. 2
 - [29] A. Sharf, T. Lewiner, G. Shklarski, S. Toledo, and D. Cohen-Or. Interactive topology-aware surface reconstruction. In *ACM Transactions on Graphics (TOG)*, volume 26, page 43. ACM, 2007. 2
 - [30] K. Siddiqi, J. Zhang, D. Macrini, A. Shokoufandeh, S. Bouix, and S. Dickinson. Retrieving articulated 3-d models using medial surfaces. *Machine vision and applications*, 19(4):261–275, 2008. 6, 8
 - [31] P. Skraba, M. Ovsjanikov, F. Chazal, and L. Guibas. Persistence-based segmentation of deformable shapes. In *Computer Vision and Pattern Recognition Workshops (CVPRW), 2010 IEEE Computer Society Conference on*, pages 45–52. IEEE, 2010. 2
 - [32] Z. Wood, H. Hoppe, M. Desbrun, and P. Schröder. Removing excess topology from isosurfaces. *ACM Transactions on Graphics (TOG)*, 23(2):190–208, 2004. 2
 - [33] K. Yin, H. Huang, H. Zhang, M. Gong, D. Cohen-Or, and B. Chen. Morfit: interactive surface reconstruction from incomplete point clouds with curve-driven topology and geometry control. 2
 - [34] Y. Zeng, D. Samaras, W. Chen, and Q. Peng. Topology cuts: A novel min-cut/max-flow algorithm for topology preserving segmentation in n-d images. *Computer vision and image understanding*, 112(1):81–90, 2008. 2
 - [35] S. Zhou, J. Changyun, and S. Lefebvre. Topology-constrained synthesis of vector patterns. *ACM Transactions on Graphics*, 33(6), 2014. 2